Progress in Nuclear Energy 172 (2024) 105213

Contents lists available at ScienceDirect

Progress in Nuclear Energy

journal homepage: www.elsevier.com/locate/pnucene

Simultaneous use of bismuth trioxide and mill scale for ternary blended geopolymer composite in radiation shielding applications

Rahul Sharma [a], Shaik Hussain [b,*], Naidu Seetala [c], John Matthews [b], Reed Edwards [b], Sudhir Amritphale [b], Elizabeth Matthews [b]

[a] *Institute for Micromanufacturing, Louisiana Tech University, Ruston, L.A 71270, USA* [b] *Trenchless Technology Center, Louisiana Tech University, Ruston, L.A 71272, USA* [c] *Department of Mathematics and Physics, Grambling State University, Grambling, LA 71245, USA*

A R T I C L E I N F O

Keywords:
Bismuth trioxide
Gamma ray shielding
Geopolymer
Mill-scale

A B S T R A C T

The present study evaluates Mill scale which is a steel industry waste and bismuth trioxide simultaneously as a potential radiation shielding material in geopolymer composite. An innovative and first of its kind lead-free design has been developed for making radiation shielding materials using mill scale and bismuth trioxide as shielding aggregates and industrial wastes such as fly ash and blast furnace slag as precursors for the geopolymer composite. The mill scale and bismuth trioxide based composite material are characterized for their radiation shielding characteristics based on shielding parameters commonly used in radiation shielding like linear attenuation coefficient (μ), half value thickness (HVT) and Mean Free Path (MVP) for 0.662 MeV energy. The determined shielding parameters are compared with traditional shielding materials like concrete with heavy aggregates. X-Ray diffraction studies have confirmed the presence of Bismuth ferrite as the major shielding phase responsible for radiation shielding. The mechanical properties of the prepared composites are determined for their strength in direct compression. Depending upon the radiation shielding parameters like linear attenuation coefficient and half value thickness an optimum dosage of mill scale and bismuth trioxide as a shielding composite to provide adequate shielding for X-Ray diagnostic and medical facilities against X-ray photons of low intensity has been recommended. The highest linear attenuation coefficient values of fly ash and slag based geopolymer composites had been observed to be 0.208 and 0.225, respectively.

1. Introduction

According to the world nuclear association sixty nuclear reactors are under construction across the world and many more are planned (Hosker, 2023; Leon, 2023), most of these are planned and are under construction in Asia. Overall, there are around 450 nuclear power plants around the world which produce about 10% of the world's total electricity. Traditionally lead had been the material of choice for radiation shielding. Later cement-based composites with hematite, magnetite, barite, lead oxide, spent lead waste etc. have been used to make radiation shielding concrete composites (Awadeen et al., 2024; Milasi et al., 2023; Gunoglu and Akkurt, 2021; Daungwilailuk et al., 2022a; Mokhtari et al., 2021; Khalil et al., 2023). For concrete to perform as an effective radiation shielding material, the thickness of concrete blocks needs to be large. Also, sometimes concrete offers poor resistance to radiation due to radiolysis of water thereby causing a loss of strength and mechanical performance (Zatloukalova et al., 2021´). As temperature increases, the strength of cement based concrete decreases and is not a desirable trait in radiation shielding (Lee et al., 2007; Mirhosseini et al., 2014). Therefore, there is a need for radiation shielding concrete which can overcome these challenges in an economically feasible and sustainable manner.

The steel industry is one of the most important industries in the world today. Steel production is an indication of the level of economic activity of the country. The annual global steel production is 1870 MT (Venkataraman et al., 2022), which results in generation of large quantities of steel industry waste. The major waste from the steel industry is red dust, iron ore fines and mill scale. Mill scale consists of hematite (Fe_2O_3), magnetite (Fe_3O_4) and wustite (FeO) phases (Ilutiu-Varvara et al., 2020). Mill scale has been used as a primary radiation shielding aggregate for making geopolymer cementitious composites for the construction sector (Kumar et al., 2021a). There are many other uses of mill scale which makes wide scale utilization of mill scale possible. Mill scale as

* Corresponding author.

E-mail addresses: rahulei166@gmail.com (R. Sharma), hussain21dec@gmail.com (S. Hussain), naidusv@gram.edu (N. Seetala), matthews@latech.edu (J. Matthews), rre014@latech.edu (R. Edwards), amritphale57@gmail.com (S. Amritphale), ematt@latech.edu (E. Matthews).

https://doi.org/10.1016/j.pnucene.2024.105213

Received 7 August 2023; Received in revised form 5 April 2024; Accepted 6 April 2024

a potential Electromagnetic interference (EMI) shielding material has also been studied in the past (Kumar et al., 2021a; Jakubas et al., 2022; Bantsis et al., 2011).

Radiation can be broadly classified into two types, ionizing radiation and non-ionizing radiation; ionizing radiation is harmful to the human body. The application of radiation technology is increasing day by day in fields such as medicine, agriculture, nuclear power plants, space technologies etc. The use of radiation is associated with harmful effects of X- ray which can have detrimental effect on the tissue and cells of the body (McBride and Schaue, 2020). The common radiation shielding materials are made using Lead and its compounds, which is expensive, heavy, and toxic in nature. According to United States Environmental Protection Agency, lead is one of the most toxic materials from both production and recycling point of view (Patrick, 2006). Hospitals and medical centres still use Lead as a primary material for radiation shielding as other radiation shielding materials are not economical and cost effective. Lead's toxicity after prolonged exposure can impact multiple systems, including reproductive, digestive, blood production, nervous, and renal, with the latter three being the most impacted (Papanikolaou et al., 2005). The development of children exposed the lead is of particular concern since children are more sensitive to lead toxicity effect and are more likely to be exposed in the environment (Papanikolaou et al., 2005; Hanna-Attisha et al., 2016). Recently, lead poisoning through contamination of the water supply in Flint, Michigan has brought to the forefront the potential that still exists with continued use of lead in certain applications (Hanna-Attisha et al., 2016). This crisis also highlights the importance of moving away from utilizing lead, where possible, to prevent future environmental exposure crises.

Apart from lead-based compounds, concrete is also used for radiation shielding materials, but are comparatively thicker than lead based materials and losses strength upon exposure to gamma radiation. Shielding concrete is made from both Ordinary Portland Cement and geopolymer binders with special additives like barite (barium sulphate) (Akkurt et al., 2010), hematite (Tekin et al., 2018), magnetite (Oto et al., 2016), barium compounds (Seenappa et al., 2017), bismuth trioxide (Halimah et al., 2019), tungsten trioxide (AbuAlRoos et al., 2020; Hosseini et al., 2022; Molina Higgins et al., 2019), nanoparticles of lead, lead oxide (Abu Saleem et al., 2023). Nanoparticles of iron and its compounds are also used for radiation shielding (Mkhaiber and Majeed, 2020). Titanium dioxide nanoparticles tend to densify the host matrix by aggregating all the molecules together and providing compactness to the overall structure (Dezhampanah et al., 2021). Boron carbide has been reported to have effectively used as a radio opaque filler in concrete (Chidiac et al., 2021). Barium based compounds have shown good shielding against gamma radiation, while also maintaining mechanical strength and not cracking due to excessive heat generated during the process (Daungwilailuk et al., 2022b). Barium based radiation shielding fillers have also been used as composite material for dental applications (Watts, 1987). Gadolinium based glass composites have been fabricated for radiation shielding for photon energies up to 662 keV (Kaewjang et al., 2014). The use of glass-based radiation shielding materials is increasing due to new and challenging demands from the defense and space industries (Sayyed and Lakshminarayana, 2018). Barite, Hematite and Magnetite based aggregates are most used for making radiation shielding concretes in either cement or geopolymer matrix. Red mud-based composites have also been prepared for radiation shielding applications which are an effective means for shielding but it is an energy intensive process, and the raw materials need to be heated in furnace till 1300 °C for the formation of the radiation shielding phases (Amritphale et al., 2007).

As the demand for nuclear energy is on rise throughout the world, the need for radiation shielding non-toxic composite which can withstand higher temperatures, needs very little to no virgin raw materials, can be industrially scalable, economically feasible and not energy intensive, is needed. The current radiation shielding concretes do not meet the desired needs. To overcome these limitations, a new radiation shielding composite that is non-toxic and has better mechanical performance upon radiation exposure is needed. This study tries to address the existing research gaps in the radiation shielding composite domain by studying geopolymer based radiation shielding concrete. The overall goal of this study is to make a radiation shielding composite which is made mostly from industrial wastes, easily available in large quantities, the process is industrially scalable that can be used for a broad spectrum of radiation shielding applications like X-Ray room shielding, bunkers, important buildings, and nuclear power plants.

While not all alternatives are non-toxic, the relatively lower toxicity or nullification of toxicity with certain radiation shielding materials compared to lead, can make their application for certain uses more advantageous. Based on the composition of the materials and literature studied so far, the authors in the present study have identified that the phases responsible for shielding are iron and iron oxides like Fe_2O_3 and Fe_3O_4 etc. Hence, Mill scale generated in millions of tons every year (Jikar and Dhokey, 2021), containing hematite (35%), magnetite (30%) phases with density 5.02 g/cc when reduced at 1100^{0}C and bismuth trioxide with density 8.93 g/cc have been used as a primary shielding aggregate in the present study.

Mill scale, which is considered a hazardous substance, contains crystalline silica, iron and iron oxides. These components can cause acute effects (respiratory, eye and skin irritation) and chronic effects to individuals with existing respiratory and skin disorders. Bismuth trioxide is not considered a hazardous substance or a probable carcinogen, and has low toxicity, but can have digestive, renal, oral and other impacts when absorption occurs or there is chronic exposure (Halimah et al., 2019; Wang et al., 2019; SDS-Safety Data Sheet, 2016). While mill scale and bismuth trioxide alone are consider toxic, these two as aggregates in radiation shielding composites in a geopolymer matrix might have reduced toxicity or even nullify it owing to the encapsulation and immobilization capacity of geopolymerisation process (Vu and Gowripalan, 2018; Zheng et al., 2010; Palacios and Palomo, 2004; Phair and Van Deventer, 2001). Heavy metals such as Pb, Cu, Cd and Cr that are found in Mill scale in less than 1%, have been reported to balance the negative charge of tetrahedral aluminium ions in unreactive zeolite and geopolymer structure due to their larger mass, smaller radius and higher valence (El-Eswed et al., 2015; Van Jaarsveld et al., 1998).

Also, as the temperature of the radiation absorbed composite can rise up to 250^{0}C (Fillmore, 2004), even though cement-based radiation shielding concretes provide good shielding at low temperatures, because they tend to crack up at higher temperatures (Khmurovska et al., 2021), geopolymer has been adopted as a shielding matrix for the study so it could sustain high temperatures. Mill scale is obtained from heat treatment by reducing hematite and magnetite and thereby has better sustenance to high temperatures as shielding aggregate in geopolymer (Yukawa et al., 2018; Oyelade et al., 2017). The presence of interfacial transition zone in cement concrete and the risk of segregation and heterogeneity in the mix due to improper compaction and transportation leading to radiation surges (ACI 304.3R-96, 2004; ACI 221R-96, 2001) makes geopolymer composite ideal for radiation shielding (Chauhan et al., 2017). Geopolymer composites are homogeneous in nature as the geopolymerization of aggregates with precursor and binder refines the interfacial transition zone in geopolymer composites over time (Demie et al., 2013) as the interfacial transition bonding between aggregate and geopolymer matrix is largely dependent on Si/Al ratio, forming Al–O–Si bonds and Na–O bonds (Kai and Dai, 2021).

2. Material properties

Industrial by-products such as Fly ash (Class F) and Blast furnace slag have been used as a basic precursor for the formulation of geopolymer composites. The activators used in the study were sodium hydroxide (12.5 M) solution and liquid sodium silicate pentahydrate (50% w/w) solution that are inorganic in nature and can sustain high temperatures. Mill scale and bismuth trioxide have been used as radiation shielding aggregates for the study. The chemical composition of the precursors used in the study are tabulated in Table 1.

The design mix proportions used in the formulation of the geopolymer composites is Tabulated in Table 2 along with the curing regime.

The geopolymer mix formulations have been designed in two-fold, the first one was to study the effect of untreated and treated mill scale in radiation shielding capacity and the second, to evaluate the dosage of bismuth trioxide in effectively shielding the radiation simultaneously with mill scale. Mill scale contained oil contamination in its raw form when received and hence was processed using various mechanisms to improve its density. Raw mill scale (untreated) was adopted in the geopolymer mix RM1. Mill scale used in mixes denoted by RM2 and RM3 have been processed and the mill scale used in remaining mixes has not been. For mix RM2, the raw mill scale was oven dried at 100^{0}C for 24 h and then ball milled for 8 h to micronize the mill scale particles. Mill scale used in mix RM3 was heated in presence of its own oil content as reducing agent at a temperature of 1100^{0}C for 1 h, cooled down to room temperature and used in the geopolymer composite. The micronizing and reduction of mill scale was performed to decrease the particle size and improve the surface area of the mill scale to enhance its shielding efficiency. In the subsequent mixes, RF1, RF2, RF3, RB1, RB2 and RB3, the mill scale was untreated, and the dosage of bismuth oxide was changed to evaluate the radiation shielding capabilities.

Cylinders of 6-inch diameter and varying thickness from 1 to 6 inch have been cast to test for the shielding efficiency and obtain linear attenuation curve. The mixes that contained Blast furnace slag in them had been cured at ambient room temperature as the presence of high amounts of lime (calcium oxide) made it highly reactive and did not need temperature activation. This was to enable ambient and in-situ casting of radiation shielding composite in the field. All the mixes with fly ash as a precursor had been cured at 70^{0}C for 24 h, demoulded and further cured at ambient room temperature. The fly ash based geopolymer mixes had been cast to enable prefabrication of the composite in the industry and ready-to-install field applications.

The dry density of the hardened geopolymer samples had been measured by calculating the ratio of mass of the sample per unit volume. The samples after their respective curing durations had been kept in the oven at 100^{0}C for 24 h to measure the dry weight. The mass of the hardened geopolymer cylinder is measured closest to 0.5 gm and the dimensions of the cylinder are calculated using vernier callipers. The ratio of mass of the sample to its volume is represented by density in gm/ cm^3.

X-ray diffraction (XRD) analysis has been performed on the mixes that yielded good shielding parameters to distinguish and identify the essential phases for improving radiation shielding efficiency of the composite using a Bruker D-8 X-ray diffractometer equipped with a Cu- K_α radiation source (1.54060 Å). The X-ray diffraction intensity was recorded as a function of Bragg's 2θ in the angular range of 10º-90º optical.

3. Methodology

3.1. Gamma radiation testing

The experimental set-up consists of a Geiger tube, a scaler or electronic counter and a radioactive source as shown in Fig. 1 (a). Radioactivity is the spontaneous decay of the nuclei of atoms. Alpha, beta, and gamma rays are the three distinct types of radiation from radioactive decay. Gamma rays have shorter wavelengths and higher energy than visible light. The Geiger Muller tube is the most widely used detector for counting radioactivity. It can detect the number of radiations emitted by a radioactive source. A Geiger Muller tube consists of a central wire in a hollow metal cylinder filled with an inert gas like argon at low pressures. A potential difference of about 700–1800 V is applied between the central wire and the cylinder so that the tube is just at the point of breaking down into an electrical discharge. An incident charged particle or gamma ray ionizes some of the gas atoms and starts a discharge. Positive ions are accelerated towards the negative cylinder and electrons are accelerated towards the central wire. The electrons attain higher velocity due to a lower effective mass. These fast-moving electrons collide with the molecules of the gas and knock out more electrons and ions, which results in a large pulse of electrons. Each pulse of electrons activates a counting circuit in the digital counter. Individual photons can be detected even when the incident flux of radiation is low. The device pulls current very quickly when it detects a radiation like gamma or beta. It makes a very short current pulse and then it counts it. A small amount of ionizing radiation can generate a large current due to the avalanche of electrons generated in the Geiger tube. The set-up uses a nucleus 500 digital counter, the internal circuitry of the Nucleus digital counter is shown in Fig. 1 (b) below. The operating potential for each Geiger tube is determined to be around 800V and set. The gamma radiation source used in the study was Cs-137 (0.662 MeV). Two overlapped Cs-137 sources, each of 5 μCi, totaling 10 μCi were used for the present study. The effect of scattering angle has been taken care of by adjusting the thickness of the sample by considering the path of direct passage of radiation in the sample, so it takes care of the angle between source and the receiver. The room radiation background is measured without the radioactive source and subtracted from each sample measurement to get the correct radiation counts. For each sample the radiation measurement is performed for 20 min in each Geiger tube.

The radiation attenuation of photons (gamma rays) by the material used under ideal conditions is given by the following equation (1).

$$I = I_0 e^{-\mu x} \quad (1)$$

Where I_0 is the intensity of the photon before hitting the material.

I is the photon intensity after the photon has passed through the material medium.

x is the thickness of the material medium in cm and μ is linear attenuation coefficient in cm^{-1}.

The gamma radiation attenuation parameters like linear attenuation coefficient, half-life thickness and tenth value thickness were determined for each composition. The thickness or layer of a shield or absorber that reduces the intensity of radiation by a factor of one half and one tenth of the initial intensity, respectively, is known as the Half-Value Thickness (HVT) and the Tenth Value Thickness (TVT). Mean Free Path (MVP), the inverse of linear attenuation coefficient (cm^{-1}) is the distance between two consecutive gamma-ray collisions that travel through a specific thickness of the shielding material has also been measured for each mix. The equations used to determine the value of half value thickness, tenth value thickness and mean free path are given below in Equations (2)–(4), respectively (Singh et al., 2018; Mansy et al., 2021; Mann et al., 2016; Mansy and Desoky, 2022).

$$HVT = \frac{\ln(2)}{\mu} \quad (2)$$

Table 1
Properties of Geopolymer precursor.

Chemical/Physical Analysis	Fly Ash (Class F)	Blast Furnace Slag
CaO	2.58%	41.41%
SiO_2	60.70%	34.20%
Al_2O_3	23.71%	13.68%
Fe_2O_3	4.73%	0.75%
MgO	1.14%	6.24%
Specific gravity	2.05	2.93
Fineness (passing 325 mesh)	78%	98%

Table 2
Design mix proportions of radiation shielding geopolymer composites (kg/m^3).

Mix notation	Fly ash	Slag	Mill scale	Bismuth trioxide	Sodium hydroxide	Sodium silicate	Curing regime
RM1	1661	0	1661	0	332	831	70⁰C 70⁰C
RM2	1661	0	1661	0	332	831	70⁰C
RM3 RF1	1661	0	1661 997	0	332	831	70⁰C
RF2	1827	0	997	498	221	554	70⁰C
RF3	1329 831	0	997	997	221	554	70⁰C
		0		1495	221	554	
RB1	0	1827	997	498	221	554	Ambient
RB2	0	1329	997	997	221	554	Ambient
RB3	0	831	997	1495	221	554	Ambient

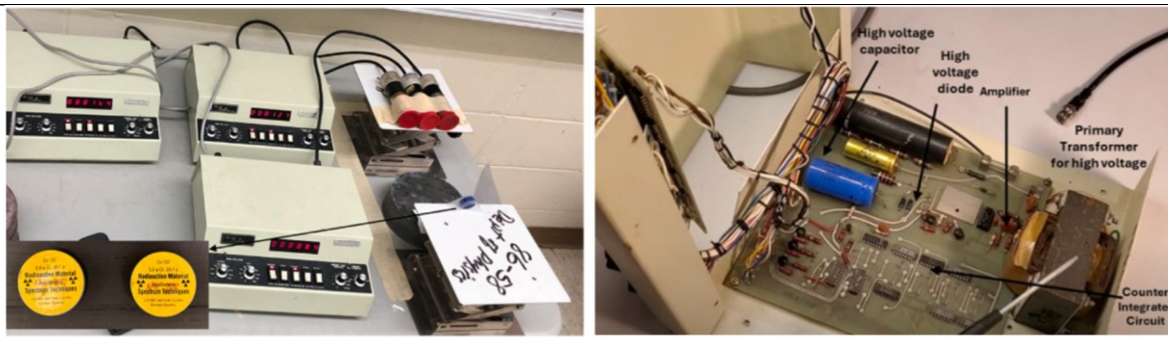

Fig. 1. (a–b). (a) Setup for gamma radiation measurement along with radiation sources (Cs-137); (b) Internal circuitry of the nucleus 500 digital radiation counter.

$$TVT = \frac{\ln(10)}{\mu} \tag{3}$$

$$MFP = \frac{1}{\mu} \tag{4}$$

3.2. Mechanical testing

To evaluate the compressive strength of the radiation shielding geopolymer composites, 2-inch cubes were prepared and cured at the same curing regimes the shielding composites were exposed to as mentioned in Table 2. The geopolymer cubes were tested as per ASTM C109 (2020) (ASTM C109, 2020) with a loading rate of 50 psi/s. Compressive strength of the cubes were also determined after their exposure to elevated temperatures of 100⁰C and 200⁰C and compared with pre-temperature exposure results.

4. Results and discussions

4.1. Radiation testing

4.1.1. Linear attenuation coefficients

Fig. 2 shows the plot of normalized counts of radiation at gamma energy of 0.662 MeV vs thickness of the radiation shielding geopolymer composite of mix RM2 in order to measure the linear attenuation coefficients. The values of linear attenuation coefficients of all the other mixes had been found similarly. The corresponding density of the composite, its Half Value Thickness (HVT), Tenth Value Thickness (TVT) and Mean Free Path (MFP) have also been calculated for each mix and tabulated in Table 3 and shown in Fig. 3. From Table 3 the minimum value of linear attenuation coefficient was observed for the mix RM1 where the shielding aggregate was untreated mill scale. Also, this mix had the highest half value thickness and tenth value thickness too. These can be attributed to the density of the hardened geopolymer composite which is the least amongst all the mixes adopted in the study. From Table 3 and it can be observed that the treatment of mill scale, both by ball-milling and by reducing at 1100⁰C yielded better attenuation

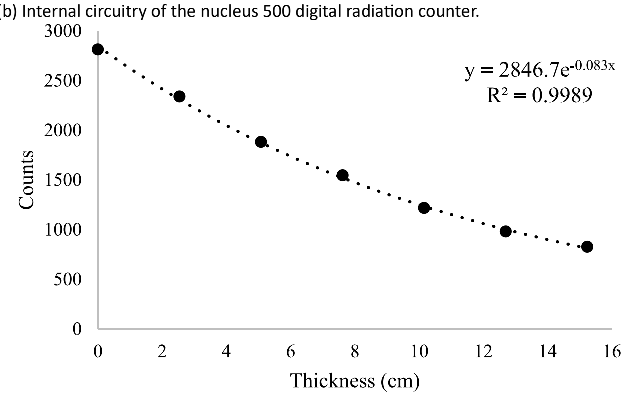

Fig. 2. Normalized counts of radiation at 662.0 keV vs thickness of the radiation shielding geopolymer composite of mix RM2.

towards radiation. This can be ascertained by the increase in the density of the geopolymer samples and by the reduction in half value and tenth value thicknesses. Ball milling the mill scale for 8 h had densified the material and provided better packing to the geopolymer matrix due to micronization of iron oxide. Heating the mill scale at 1100⁰C had used the oils as reducing agent and enhanced its density. This resulted in the formation of new phases Fig. 3 such as Wustite (FeO) and Fe which had more density compared to Magnetite and Hematite from untreated mill scale as seen in the XRD results in the proceeding section.

Mixes with bismuth trioxide included in the geopolymer concrete along with untreated mill scale showed better resistance to radiation. The value of linear attenuation coefficients decreased with the increase in the dosage of bismuth trioxide, again attributed to the increase in the density of the composite. Slag based geopolymer composites cured at ambient temperature performed better than the geopolymer composites based out of fly ash. This is due to slag having more specific gravity compared to the fly ash (Hasan et al., 2021). Also, the formation of calcites and calcium-silicate-hydrates (C–S–H gel) densified the slag

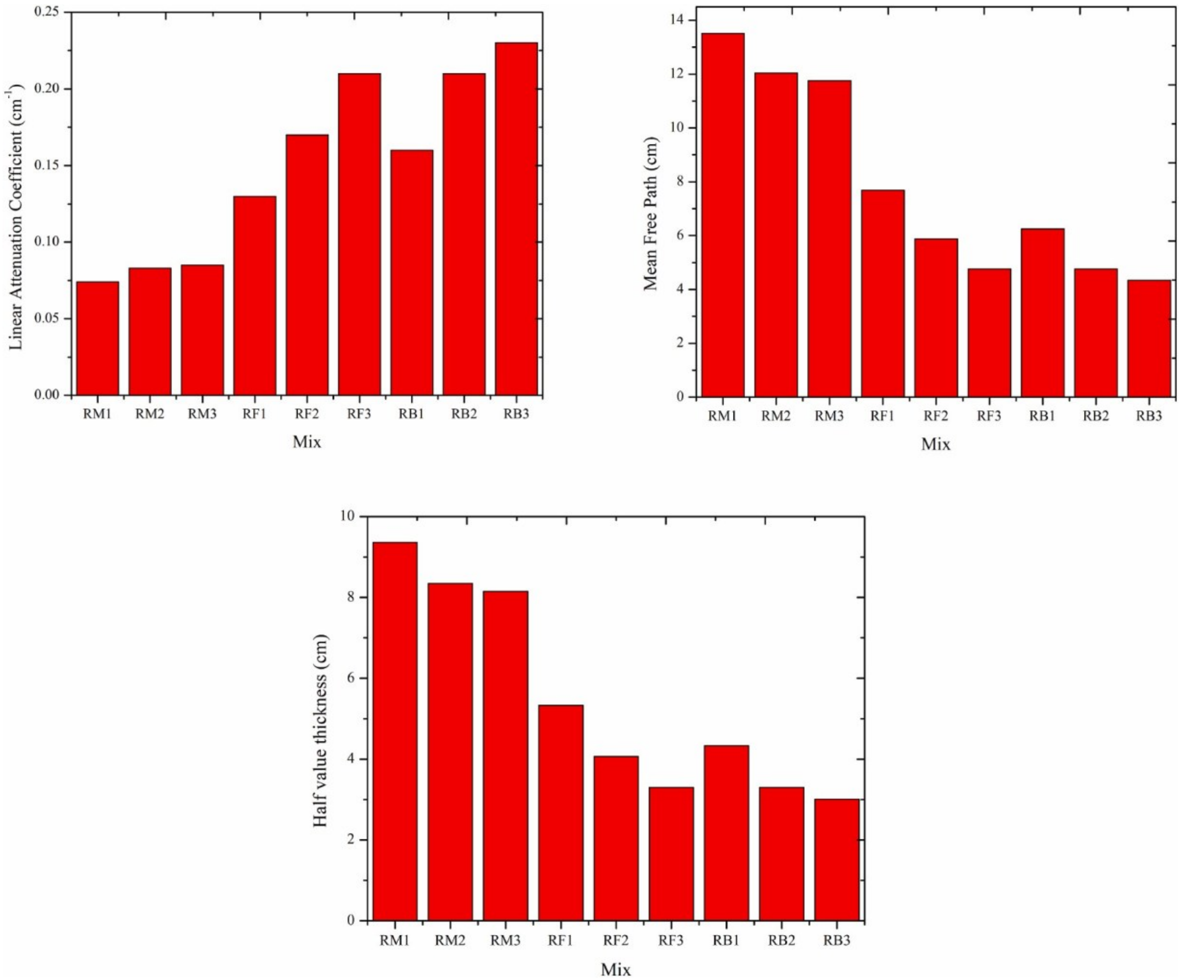

Fig. 3. Plot of Linear Attenuation Coefficient, Mean Free Path, and Half Value Thickness of the mixes.

Table 3
Linear Attenuation coefficient, half value thickness, tenth value thickness at 662.0 keV gamma radiation energy.

Mix	μ (cm^{-1})	HVT (cm)	TVT (cm)	Mean free path (cm)	Density (g/cm^3)
RM1	0.074	9.36	31.11	13.51	1.52
RM2	0.083	8.35	27.74	12.04	1.80
RM3	0.085	8.15	27.08	11.76	2.02
RF1	0.131	5.33	17.71	7.69	2.08
RF2	0.170	4.07	13.54	5.88	2.26
RF3	0.213	3.30	10.96	4.76	2.57
RB1	0.163	4.33	14.39	6.25	2.33
RB2	0.214	3.30	10.96	4.76	2.64
RB3	0.231	3.01	10.01	4.34	2.69

based geopolymer matrix providing slightly more shielding efficiency compared to the fly ash based geopolymer composites.

4.1.2. Validation of radiological parameters using Phy-X-PSD

A user-friendly online software for predicting radiation shielding parameters and dosimetry has been used to validate the results obtained through experimental analysis (Şakar et al., 2020). The details of molar fractions and density of the hardened geopolymer samples had been used as input parameters to predict the values of linear attenuation coefficient, half value thickness and mean free path. The software could also generate data on shielding parameters in the continuous energy range from 1 keV to 100 GeV (Desoky et al., 2023). Table 4 shows the comparison of experimental and predicted radiological parameters.

4.1.3. Transmittance of geopolymer composites

The values of Transmittance (%) in accordance with thickness of geopolymer composite obtained from the Linear Attenuation data is plotted in Fig. 4. From the curve it is seen that the density of composite is inversely proportional to the radiation energy received by the sample. As the thickness increased, the transmittance had decreased exponentially. The exponential decrease in the plot of the mixes with bismuth trioxide (RF1, RF2, RF3, RB1, RB2 and RB3) is more significant than the mixes without bismuth trioxide (RM1, RM2 and RM3). The higher the gradient of the plot (Linear Attenuation Coefficient), deeper is the curve as seen for mix RB3 indicating the best radiation resistance for this sample.

4.1.4. Density of the composites

The density of the composites is greatly dependent on the relative density of the shielding aggregates and the dosage of the aggregates in making the composite. A linear proportionality has been observed between the density of the composite and the linear attenuation coefficient values. Fig. 5 shows the correlation between density and linear attenuation of coefficient of the geopolymer composites from various literature (Hasan et al., 2021; Tahir et al., 2019; Kumar et al., 2021b; Khater et al., 2021; Ouda, 2021) and compared with the present study. The source of energy for all the values plotted in the curve in Fig. 5 is from Cs-137 source with photon energy of 0.662 MeV. Tahir et al. (2019) (Tahir et al., 2019) formulated a fly ash based geopolymer with graphite and iron oxide as shielding aggregates to study the radiation attenuation of the composite. Hasan et al. (2021) (Hasan et al., 2021) in their study based on nickel slag and fly ash geopolymer deduced that slag based

Table 4
Comparison of radiological parameters from experimental and software analysis at 662.0 keV gamma radiation energy.

Mix	μ (cm^{-1})		HVT (cm)		MFP (cm)	
	Experimental	Phy-X-PSD	Experimental	Phy-X-PSD	Experimental	Phy-X-PSD
RM1	0.074	0.091	9.36	7.60	13.51	11.01
RM2	0.083	0.095	8.35	7.32	12.04	10.55
RM3	0.085	0.099	8.15	7.10	11.76	10.15
RF1	0.131	0.167	5.33	4.14	7.69	5.98
RF2	0.170	0.191	4.07	3.62	5.88	5.23
RF3	0.213	0.228	3.30	3.03	4.76	4.39
RB1	0.163	0.188	4.33	3.70	6.25	5.33
RB2	0.214	0.224	3.30	3.10	4.76	4.45
RB3	0.231	0.239	3.01	2.90	4.34	4.20

The trend in the variations in all three parameters, linear attenuation coefficient, half value thickness, and mean free path, agrees between experimental and Phy-X-PSD software analysis with Phy-X-PSD slightly overestimating the linear attenuation coefficient and underestimating the half value thickness and mean free path for all sample. Both experimental and Phy-X-PSD software analysis showed RB3, mix with bismuth trioxide included in the geopolymer concrete along with untreated mill scale, showed the best resistance to radiation.

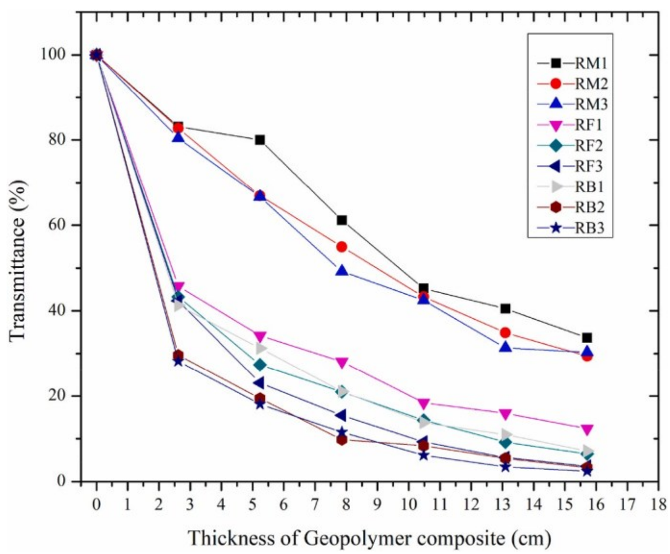

Fig. 4. Correlation between Thickness of Geopolymer composite vs Transmittance.

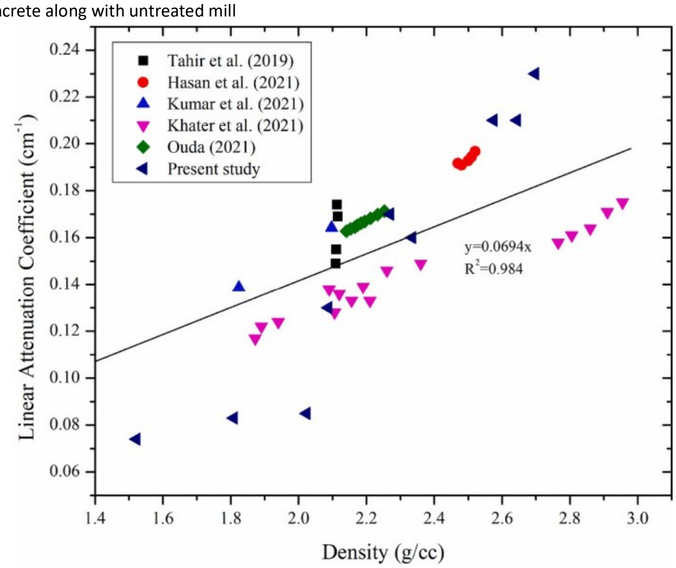

Fig. 5. Correlation between density of geopolymer composite and its linear attenuation coefficient.

geopolymer composites without any additional shielding aggregates had better shielding capacity due to the high specific gravity of nickel slag compared to fly ash. In a similar study, Kumar et al. (2021) (Kumar et al., 2021b) concluded that the slag-based hybrid geopolymer with bismuth trioxide as aggregate and slag partially replacing cement had more density and shielding capacity compared to cement concrete and lead based fly ash concrete. Electric Arc Furnace Slag (EAFS) is also observed to have been enhanced the density and thereby the shielding capacity of the geopolymer composites (Khater et al., 2021). A blend of EAFS and blast furnace slag with lead slag as aggregate gave the most efficient geopolymer composite in a study conducted by Khater et al. (2021) (Khater et al., 2021). Concrete waste containing dolomite ore with fly ash as a precursor also yielded a high density geopolymer composite with radiation shielding capabilities (Ouda, 2021).

Of all the studies mentioned in Fig. 5, the slope of values from the present study based out of ternary blend of bismuth trioxide and mill scale geopolymer had yielded better attenuation as bismuth has larger nuclear size, higher atomic number and electron density providing for increased interaction between radiation and shielding matrix delivering better shield against gamma radiation.

4.2. Compressive strength

The compressive strength of the geopolymer composites have been measured using cubes of 2 inch. The geopolymer cubes have been cured under the same conditions as that of samples used to radiation testing. In addition, geopolymer cubes have been exposed to an elevated temperature of 100⁰C and 200⁰C at a rate of 5⁰C/min for an hour and cooled down to room temperature, prior to their test in compression. The results of compression test and the plot for all the mixes are shown in Fig. 6.

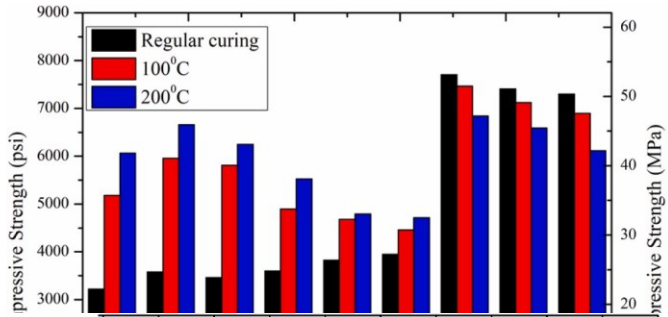

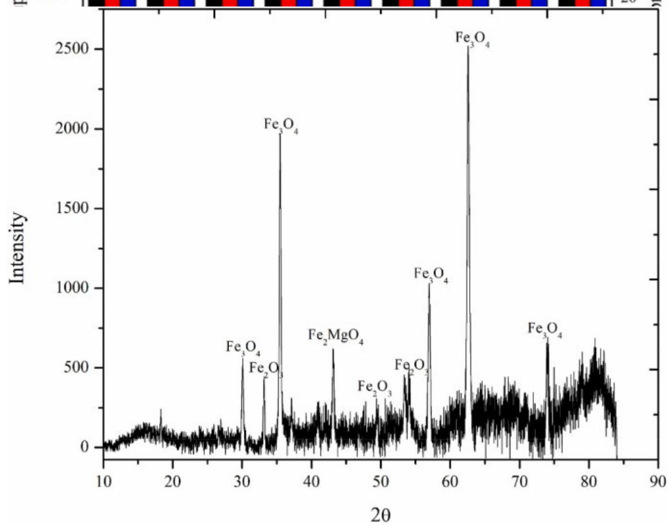

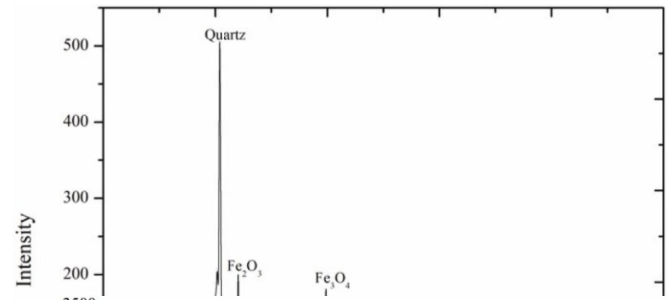

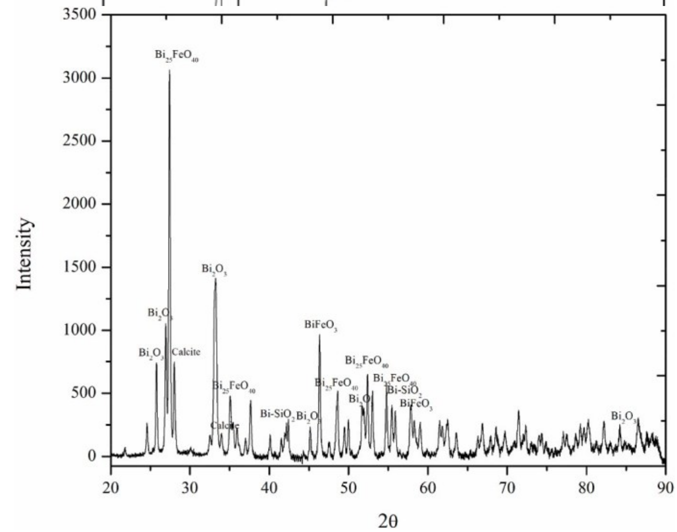

Fig. 7. XRD spectra of Raw Mill Scale.

Fig. 8. XRD spectra of Reduced mill scale geopolymer composite (RM3).

The geopolymer mixes that are fly ash based (RM1, RM2, RM3, RF1, RF2 and RF3) displayed an increase in the compressive strength when subjected to elevated temperatures due to the additional geopolymerization process. Autoclaving conditions and gas pore pressure may arise due to the conversion of moisture into vapor triggering an additional geopolymerization. The fly-ash based samples are more porous in structure and thereby can effectively resist vapor pressure build-up (Pan et al., 2009). Samples of mix with blast furnace slag as a precursor displayed an early increase in the compressive strength due to the formation of calcium based geopolymer products such as calcium silicate hydrates and calcium alumino-silicate hydrates. At elevated temperatures, due to dehydration and decomposition of calcium carbonates these bonds are broken resulting in crack propagation and eventual decrease in compressive strength (Pan et al., 2018).

Fig. 6. Compressive strength of geopolymer samples at curing temperature, 100⁰C and 200⁰C.

4.3. *Microstructural analysis*

The X-Ray diffraction results of raw mill scale (unprocessed) as received was studied and the phase changes have been compared with the geopolymer composite with reduced (heated at 1100⁰C) mill scale. Fig. 7 shows the XRD plot of raw mill scale with presence of Magnetite (Fe_3O_4) and Hematite (Fe_2O_3) as major phases. When the mill scale was reduced at 1100⁰C and used in the geopolymer formulation, the dominant phases were Wustite (FeO) and Fe as seen in Fig. 8. The density of Magnetite and Hematite were 5.17 g/cc and 5.24 g/cc, respectively; whereas the density of Wustite and Fe were 5.74 g/cc and 7.87 g/cc, respectively. This explains the increase in the density and shielding efficiency of RM3 composite when compared to RM1 and RM2.

The XRD plots of geopolymer samples of mixes RF3 and RB3 are shown in Figs. 9 and 10, respectively. From both the XRD plots, Bismuth Ferrite ($BiFeO_3$) has been observed as one of the phases apart from $Bi_{25}FeO_{40}$ and $Bi_2Fe_4O_9$. The density of Bismuth Ferrite is 8.22 g/cc and that of $Bi_2Fe_4O_9$ is 6.51 g/cc and are collectively responsible for the increase in the density of composite and its shielding efficiency, although, the sample containing blast furnace slag as a precursor had other phases such as calcite that are responsible for the matrix densification. Traces of Bi–SiO_2 have also been observed in both the samples.

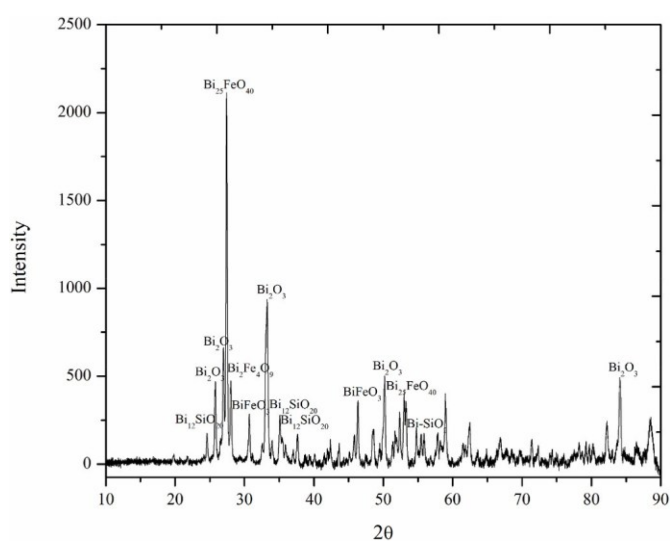

Fig. 9. XRD spectra of sample from Mix RF3.

Fig. 10. XRD spectra of sample from Mix RB3.

4.4. *Comparison with radiation shielding concrete*

Compared to the previous studies conducted in this field, the present study uses lead free materials from industrial waste ensuring constant availability of raw materials for commercial production of radiation shielding composites. Most of the raw materials used in this study are easily available in large quantities hence suitable for commercial production. It is not an energy intensive process unlike red mud-based radiation shielding composites where the raw materials need a heating up to 1300 °C to achieve radiation shielding phases (Amritphale et al., 2007). Compared to the cement-based radiation shielding composites, geopolymer based radiation shielding composites can withstand higher temperatures, are non-toxic, corrosion resistant, industrially scalable, higher linear attenuation coefficient, and less thickness needed for shielding the radiation.

The relation between density and the linear attenuation coefficient for concrete follows a similar linear relation as that of geopolymer composites. For the photon energy used in the present study, 0.662 MeV, the comparisons of linear attenuation coefficients for various grades of concrete with slag-based mill scale & bismuth trioxide geopolymer composite used in the present study are listed in Table 5. It can be seen in the comparison that the geopolymer composite formulated in the present study performed better in terms of radiation shielding when compared to concrete with heavy aggregates such as barite, hematite.

The linear attenuation coefficient values of the bismuth trioxide-mill scale geopolymer developed in the present study are better (0.23 cm-1) compared to highly used, toxic lead-based radiation shielding concrete as can be seen from Tables 4 and 5 This is due to the addition of bismuth trioxide in silicate-based glass giving Bi–SiO_2 phases as observed in Figs. 9 and 10, which gives a higher density matrix and shows better shielding properties when compared to lead-silicate-based glass (Chandraboss et al., 2015).

5. Conclusion

The current paper presented a fly ash and slag based geopolymer composites with Mill-scale and bismuth trioxide as shielding aggregates. The radiation shielding capabilities of the composites and their compressive strength have been measured. Following conclusions have been drawn from the study.

i. Among geopolymer composites which had only mill scale as aggregate, the sample where mill scale has been reduced using its own oil contaminant at 1100^{0}C (Mix RM3) performed best in terms of radiation shieling efficiency and its transmittance.
ii. Although the radiation shielding of the mix RM3 was best among only mill scale as aggregate, the compressive strength of the mix RM2 was highest at curing temperature and at elevated temperatures. Ball milling the mill scale reduced the particle size of the mill scale to nano size and hence provided better particle packing for resistance in compression.
iii. Fly ash based geopolymer with both mill scale and bismuth trioxide yielded better compressive strength upon heating at elevated temperatures. The increase in the strength was around 36% and 53% at 100^{0}Cand 200^{0}C, respectively for mix RF3. The radiation shielding properties of these mixes were relatively less efficient compared to the slag based geopolymer counterpart. iv. Slag based geopolymer composite with mill scale and bismuth trioxide where the percentage weight of bismuth trioxide was highest (mix RB3) gave the best radiation shielding efficiency due to highest density and formation of bismuth ferrite phase. The specific gravity of slag compared to fly ash is more and therefore has also played a key role in enhancing the density of this mix.
v. Slag based geopolymer composite has slightly decreased compressive strength at elevated temperatures, 5.5% decrease at 100^{0}C and 16% decrease at 200^{0}C, although the decreased strength is still well high above the required strength of mortar as per standards. vi. The initial strength of slag based geopolymer composite prior to exposure to elevated temperature was still significantly more (2.14–2.4 times) than that fly ash based geopolymer composite prior to its exposure to elevated temperature.

Table 5
Linear Attenuation Coefficient values of Radiation Shielding Concrete at 662.0 keV gamma radiation energy.

S/ No	Authors	Type of Concrete	Linear Attenuation Coefficient (cm^{-1})
1	Singh et al. (2015) (Singh et al., 2015a)	Fly ash Portland Pozzolana concrete	0.167
2	Singh et al. (2015) (Singh et al., 2015b)	Fly ash concrete with Lead	0.201
3	Singh et al. (2015) (Singh et al., 2015b)	Diaspore fly ash concrete	0.127
4	Azreen et al. (2020) (Azreen et al., 2020)	Barite based Ultra-high-performance concrete	0.208
5	Gencel et al. (2021) (Gencel et al., 2011)	Hematite loaded concrete	0.219

CRediT authorship contribution statement

Rahul Sharma: Writing – original draft, Investigation, Formal analysis, Data curation. **Shaik Hussain:** Writing – original draft, Software, Investigation, Formal analysis, Data curation. **Naidu Seetala:** Supervision, Resources, Methodology, Conceptualization. **John Matthews:** Supervision, Resources, Project administration. **Reed Edwards:** Writing – review & editing, Formal analysis. **Sudhir Amritphale:** Writing – review & editing, Visualization, Supervision, Methodology, Formal analysis, Conceptualization. **Elizabeth Matthews:** Writing – review & editing, Validation, Methodology.

Declaration of competing interest

The authors declare that they have no known competing financial interests or personal relationships that could have appeared to influence the work reported in this paper.

Data availability

Data will be made available on request.

References

Abu Saleem, R., Abdelal, N., Alsabbagh, A., Al-Jarrah, M., Al-Jawarneh, F., 2023. Effect of lead nanoparticles on the radiation shielding characteristics of carbon fiber/epoxy composites. J. Reinforc. Plast. Compos. 42 (9–10), 483–493.
AbuAlRoos, N.J., Azman, M.N., Amin, N.A.B., Zainon, R., 2020. Tungsten-based material as promising new lead-free gamma radiation shielding material in nuclear medicine. Phys. Med. 78, 48–57.
ACI 221R-96, 2001. Guide for Use of Normal Weight and Heavyweight Aggregates in Concrete Reported by ACI Committee 221. Detroit, MI.
ACI 304.3R-96, 2004. Heavyweight Concrete: Measuring, Mixing, Transporting, and Placing Reported by ACI Committee 304. Detroit, MI.
Akkurt, I., Akyildirim, H., Mavi, B., Kilincarslan, S., Basyigit, C., 2010. Gamma-ray shielding properties of concrete including barite at different energies. Prog. Nucl. Energy 52 (7), 620–623.
Amritphale, S.S., Anshul, A., Chandra, N., Ramakrishnan, N., 2007. A novel process for making radiopaque materials using bauxite—red mud. J. Eur. Ceram. Soc. 27 (4), 1945–1951.
ASTM C109, 2020. Standard Test Method for Compressive Strength of Hydraulic Cement Mortars (Using 2-in. Or [50-mm] Cube Specimens).
Awadeen, M., Amin, M., Bakr, R.H., Tahwia, A.M., 2024. Mechanical properties, attenuation coefficient, and microstructure of ultra high-performance heavyweight concrete for radiation shielding applications. J. Build. Eng. 82, 108395.
Azreen, N.M., Rashid, R.S., Amran, Y.M., Voo, Y.L., Haniza, M., Hairie, M., et al., 2020. Simulation of ultra-high-performance concrete mixed with hematite and barite aggregates using Monte Carlo for dry cask storage. Construct. Build. Mater. 263, 120161.
Bantsis, G., Sikalidis, C., Betsiou, M., Yioultsis, T., Xenos, T., 2011. Electromagnetic absorption, reflection and interference shielding in X-band frequency range of low cost ceramic building bricks and sandwich type ceramic tiles using mill scale waste as an admixture. Ceram. Int. 37 (8), 3535–3545.
Chandraboss, V.L., Kamalakkannan, J., Senthilvelan, S., 2015. Synthesis of AC-Bi@ SiO2 nanocomposite sphere for superior photocatalytic activity towards the photodegradation of malachite green. Canadian Chemical Transactions 3 (4), 410–429.
Chauhan, R.K., Mudgal, M., Verma, S., Amritphale, S.S., Das, S., Shrivastva, A., 2017. Development and design mix of radiation shielding concrete for gamma-ray shielding. J. Inorg. Organomet. Polym. Mater. 27, 871–882.
Chidiac, S.E., El-Samrah, M.G., Reda, M.A., Abdel-Rahman, M.A.E., 2021. Mechanical and radiation shielding properties of concrete containing commercial boron carbide powder. Construct. Build. Mater. 313, 125466.
Daungwilailuk, T., Yenchai, C., Rungjaroenkiti, W., Pheinsusom, P., Panwisawas, C., Pansuk, W., 2022a. Use of barite concrete for radiation shielding against gamma- rays and neutrons. Construct. Build. Mater. 326, 126838.

Daungwilailuk, T., Yenchai, C., Rungjaroenkiti, W., Pheinsusom, P., Panwisawas, C., Pansuk, W., 2022b. Use of barite concrete for radiation shielding against gamma- rays and neutrons. Construct. Build. Mater. 326, 126838.

Demie, S., Nuruddin, M.F., Shafiq, N., 2013. Effects of micro-structure characteristics of interfacial transition zone on the compressive strength of self-compacting geopolymer concrete. Construct. Build. Mater. 41, 91–98.

Desoky, W.M., Mansy, M.S., 2023. Dielectric, conductivity properties, elastic moduli, and gamma-ray attenuation abilities: a wide-ranging investigation into Molybdenum added ferrite nanoparticles. Phys. Scripta 99 (1), 015907.

Dezhampanah, S., Nikbin, I.M., Mehdipour, S., Mohebbi, R., Moghadam, H., 2021. Fiber-reinforced concrete containing nano-TiO2 as a new gamma-ray radiation shielding materials. J. Build. Eng. 44, 102542.

El-Eswed, B.I., Yousef, R.I., Alshaaer, M., Hamadneh, I., Al-Gharabli, S.I., Khalili, F., 2015. Stabilization/solidification of heavy metals in kaolin/zeolite based geopolymers. Int. J. Miner. Process. 137, 34–42.

Fillmore, D.L., 2004. Literature Review of the Effects of Radiation and Temperature on the Aging of Concrete.

Gencel, O., Bozkurt, A., Kam, E., Korkut, T., 2011. Determination and calculation of gamma and neutron shielding characteristics of concretes containing different hematite proportions. Ann. Nucl. Energy 38 (12), 2719–2723.

Gunoglu, K., Akkurt, I., 2021. Radiation shielding properties of concrete containing magnetite. Prog. Nucl. Energy 137, 103776.

Halimah, M.K., Azuraida, A., Ishak, M., Hasnimulyati, L., 2019. Influence of bismuth oxide on gamma radiation shielding properties of boro-tellurite glass. J. Non-Cryst. Solids 512, 140–147.

Hanna-Attisha, M., LaChance, J., Sadler, R.C., Champney Schnepp, A., 2016. Elevated blood lead levels in children associated with the Flint drinking water crisis: a spatial analysis of risk and public health response. Am. J. Publ. Health 106 (2), 283–290.

Hasan, M.W., Sugiharto, S., Astutiningsih, S., 2021. Gamma radiation shielding properties of slag and fly ash-based geopolymers. At. Indones. 47 (3), 173–180.

Hosker, E., 2023. World Energy Outlook 2023, Directorate of Sustainability, Technology and Outlooks. International Energy Agency.

Hosseini, M.A., Malekie, S., Kazemi, F., 2022. Experimental evaluation of gamma radiation shielding characteristics of polyvinyl alcohol/tungsten oxide composite: a comparison study of micro and nano sizes of the fillers. In: Nuclear Instruments and Methods in Physics Research Section A: Accelerators, Spectrometers, Detectors and Associated Equipment, vol. 1026, 166214.

Ilutiu-Varvara, D.A., Tintelecan, M., Aciu, C., Sas-Boca, I.M., 2020. Reuse of the steel mill scale for sustainable industrial applications. Multidisciplinary Digital Publishing Institute Proceedings, vol. 63, 14.

Jakubas, A., Łada-Tondyra, E., Makowka, M., Suchecki,´ Ł., 2022. A study on the possibility of using iron scale in the construction of electromagnetic field shields. Energies 15 (4), 1332.

Jikar, P.C., Dhokey, N.B., 2021. Overview on production of reduced iron powder from mill scale waste. Mater. Today: Proc. 44, 4324–4329.

Kaewjang, S., Maghanemi, U., Kothan, S., Kim, H.J., Limkitjaroenporn, P., Kaewkhao, J., 2014. New gadolinium based glasses for gamma-rays shielding materials. Nucl. Eng. Des. 280, 21–26.

Kai, M.F., Dai, J.G., 2021. Understanding geopolymer binder-aggregate interfacial characteristics at molecular level. Cement Concr. Res. 149, 106582.

Khalil, M.S., Arab, M.A.E.S., Etman, A.E., Abdelwahab, N.R., Moustafa, W.M., Hamouda, A.S., 2023. Experimental and theoretical investigation for shielding efficiency of self-compacted concrete containing lead smelting waste for gamma ray. Case Stud. Constr. Mater. 19, e02401.

Khater, H.M., Ramadan, W., Gharieb, M., 2021. Impact of alkali activated mortar incorporating different heavy metals on immobilization proficiency using gamma rays attenuation. Prog. Nucl. Energy 137, 103729.

Khmurovska, Y., Stemberk, P., Sikorin, S., Nemˇ eˇcek, J., Jo´´zwiak-Nied´zwiedzka, D., Doleˇzelova, M., et al., 2021. Effects of gamma-ray irradiation on hardened cement´ mortar. International Journal of Concrete Structures and Materials 15, 1–14.

Kumar, N., Amritphale, S.S., Matthews, J.C., Lynam, J.G., Alam, S., Abdulkareem, O.A., 2021a. Synergistic utilization of diverse industrial wastes for reutilization in steel production and their geopolymerization potential. Waste Management 126, 728–736.

Kumar, S., Mann, K.S., Singh, T., Singh, S., 2021b. Investigations on the gamma-ray shielding performance of green concrete using theoretical, experimental and simulation techniques. Prog. Nucl. Energy 134, 103654.

Lee, C.M., Lee, Y.H., Lee, K.J., 2007. Cracking effect on gamma-ray shielding performance in concrete structure. Prog. Nucl. Energy 49 (4), 303–312.

Leon, S.B., 2023. World nuclear performance Report 2023. World Nuclear Association 2023/001.

Mann, H.S., Brar, G.S., Mudahar, G.S., 2016. Gamma-ray shielding effectiveness of novel light-weight clay-flyash bricks. Radiat. Phys. Chem. 127, 97–101.

Mansy, M.S., Desoky, W.M., 2022. Investigation of gamma-rays and fast neutrons attenuation parameters for NixCo1-xFe2O4 nickel ferrites. Prog. Nucl. Energy 148, 104213.

Mansy, M.S., Lasheen, Y.F., Breky, M.M., Selim, Y., 2021. Experimental and theoretical investigation of Pb–Sb alloys as a gamma-radiation shielding material. Radiat. Phys. Chem. 183, 109416.

McBride, W.H., Schaue, D., 2020. Radiation-induced tissue damage and response. J. Pathol. 250 (5), 647–655.

Milasi, S.E., Mostofinejad, D., Bahmani, H., 2023. Improving the resistance of ultra-high-performance concrete against nuclear radiation: replacing cement with Barite, hematite, and lead powder. Developments in the Built Environment 15, 100190.

Mirhosseini, S., Polak, M.A., Pandey, M., 2014. Nuclear radiation effect on the behavior of reinforced concrete elements. Nucl. Eng. Des. 269, 57–65.

Mkhaiber, A.F., Majeed, A.M.A., 2020. The effect of using Nano iron oxide in radiological shielding. In: IOP Conference Series: Materials Science and Engineering, vol. 928. IOP Publishing, 072033, 7.

Mokhtari, K., Saadi, M.K., Ahmadpanahi, H., Jahanfarnia, G., 2021. Fabrication, characterization, simulation and experimental studies of the ordinary concrete reinforced with micro and nano lead oxide particles against gamma radiation. Nucl. Eng. Technol. 53 (9), 3051–3057.

Molina Higgins, M.C., Radcliffe, N.A., Toro-Gonzalez, M., Rojas, J.V., 2019. Gamma ray´ attenuation of hafnium dioxide-and tungsten trioxide-epoxy resin composites. J. Radioanal. Nucl. Chem. 322, 707–716.

Oto, B., Gür, A., Kavaz, E., Çakır, T., Yaltay, N., 2016. Determination of gamma and fast neutron shielding parameters of magnetite concretes. Prog. Nucl. Energy 92, 71–80.

Ouda, A.S., 2021. A preliminary investigation on gamma-rayattenuation of alkali- activated concrete waste based-geopolymer modified with pozzocrete-fly ash. Prog. Nucl. Energy 134, 103681.

Oyelade, A.O., Odegbaro, D.O., Fapohunda, C.A., 2017. Effect of elevated temperature on the compressive strength of concrete produced with pulverized steel mill scale. Nigerian Journal of Technology 36 (4), 1030–1034.

Palacios, M., Palomo, A., 2004. Alkali-activated fly ash matrices for lead immobilisation: a comparison of different leaching tests. Adv. Cement Res. 16 (4), 137–144.

Pan, Z., Sanjayan, J.G., Rangan, B.V., 2009. An investigation of the mechanisms for strength gain or loss of geopolymer mortar after exposure to elevated temperature. J. Mater. Sci. 44, 1873–1880.

Pan, Z., Tao, Z., Cao, Y.F., Wuhrer, R., Murphy, T., 2018. Compressive strength and microstructure of alkali-activated fly ash/slag binders at high temperature. Cement Concr. Compos. 86, 9–18.

Papanikolaou, N.C., Hatzidaki, E.G., Belivanis, S., Tzanakakis, G.N., Tsatsakis, A.M., 2005. Lead toxicity update. A brief review. Med. Sci. Mon. Int. Med. J. Exp. Clin. Res. 11 (10), RA329.

Patrick, L., 2006. Lead toxicity, a review of the literature. Part I: exposure, evaluation, and treatment. Alternative Med. Rev. 11 (1).

Phair, J.W., Van Deventer, J.S.J., 2001. Effect of silicate activator pH on the leaching and material characteristics of waste-based inorganic polymers. Miner. Eng. 14 (3), 289–304.

S¸akar, E., Ozpolat, ¨ O.F., Alım, B., Sayyed, M.I., Kurudirek, M., 2020. Phy-X/PSD: ¨ development of a user-friendly online software for calculation of parameters relevant to radiation shielding and dosimetry. Radiat. Phys. Chem. 166, 108496.

Sayyed, M.I., Lakshminarayana, G., 2018. Structural, thermal, optical features and shielding parameters investigations of optical glasses for gamma radiation shielding and defense applications. J. Non-Cryst. Solids 487, 53–59.

[Online] SDS-safety Data Sheet: Bismuth Trioxide, 2016. Puritan Products. puritanproducts.com/wp-content/uploads/2015/08/BISMUTH-TRIOXIDE-SDS.pdf. (Accessed 31 July 2023).

Seenappa, L., Manjunatha, H.C., Chandrika, B.M., Chikka, H., 2017. A study of shielding properties of X-ray and gamma in barium compounds. Journal of Radiation Protection and Research 42 (1), 26–32.

Singh, K., Singh, S., Dhaliwal, A.S., Singh, G., 2015a. Gamma radiation shielding analysis of lead-flyash concretes. Appl. Radiat. Isot. 95, 174–179.

Singh, K., Singh, S., Singh, S.P., Mudahar, G.S., Dhaliwal, A.S., 2015b. Gamma radiation shielding and health physics characteristics of diaspore-flyash concretes. J. Radiol. Prot. 35 (2), 401.

Singh, T., Kaur, A., Sharma, J., Singh, P.S., 2018. Gamma rays' shielding parameters for some Pb-Cu binary alloys. Engineering science and technology, an international journal 21 (5), 1078–1085.

Tahir, D., Abdullah, B., Ansar, A., Ilyas, S., Mutmainna, I., Madda, W.I., 2019. Geopolimer concrete for radiation shielding application. In: Materials Science Forum, vol. 966. Trans Tech Publications Ltd, pp. 41–47.

Tekin, H.O., Sayyed, M.I., Issa, S.A., 2018. Gamma radiation shielding properties of the hematite-serpentine concrete blended with WO3 and Bi2O3 micro and nano particles using MCNPX code. Radiat. Phys. Chem. 150, 95–100.

Van Jaarsveld, J.G.S., Van Deventer, J.S.J., Lorenzen, L.L., 1998. Factors affecting the immobilization of metals in geopolymerized flyash. Metall. Mater. Trans. B 29, 283–291.

Venkataraman, M., Csereklyei, Z., Aisbett, E., Rahbari, A., Jotzo, F., Lord, M., Pye, J., 2022. Zero-carbon steel production: the opportunities and role for Australia. Energy Pol. 163, 112811.

Vu, T.H., Gowripalan, N., 2018. Mechanisms of heavy metal immobilisation using geopolymerisation techniques–A review. J. Adv. Concr. Technol. 16 (3), 124–135.

Wang, R., Li, H., Sun, H., 2019. Bismuth: Environmental Pollution and Health Effects, Zatloukalova, J., Dewynter-Marty, V., Zatloukal, J., Ko´ la´ˇr, K., Hlava´ˇc, Z., Guillot, W., vol. 415. Encyclopedia of environmental health. Konvalinka, P., 2021. Investigation of radiolysis in cement pastes immobilizing Watts, D.C., 1987. Radiopacity vs. composition of some barium and strontium glass simulated evaporator concrentrates. Ann. Nucl. Energy 151, 107901.

composites. J. Dent. 15 (1), 38–43. Zheng, L., Wang, W., Shi, Y., 2010. The effects of alkaline dosage and Si/Al ratio on the Yukawa, N., Abe, E., Fujiwara, S., 2018. Thermal properties of oxide scale on surface of immobilization of heavy metals in municipal solid waste incineration fly ash-based work roll in hot rolling mill. Procedia Manuf. 15, 59–64. geopolymer. Chemosphere 79 (6), 665–671.